Thermal annealing dependence of some physical properties of Bi-substituted Sn–Sb–Se glassy thin films

M. Ahmad[1], R. Thangaraj[1,a], and T.S. Sathiaraj[2]

[1] Semiconductors Laboratory, Department of Applied Physics, Guru Nanak Dev University, Amritsar, 143005 Punjab, India
[2] Department of Physics, University of Botswana, Botswana

Received: 10 March 2009 / Accepted: 23 March 2009
Published online: 10 June 2009 – © EDP Sciences

Abstract. Bulk glasses of the $Sn_{10}Sb_{20-x}Bi_xSe_{70}$ ($0 \leqslant x \leqslant 8$) system were prepared by the conventional melt quenching technique. Thin films were prepared by the thermal evaporation technique on glass substrates. Appearance of some crystalline phases is observed from the X-ray diffractograms after heat treatment below the glass transition temperature for 1 h. Scanning electron microscopy studies also show the presence of microcrystalline phases in the amorphous matrix after annealing for 1 h. The effect of Bi concentration and heat treatment on the optical gap and activation energy for dark conductivity were also investigated for the pristine as well as annealed films. The results are discussed on the basis of models related to the presence of defect states in chalcogenide materials.

PACS. 61.05.C- X-ray diffraction and scattering – 68.37.-d Microscopy of surfaces, interfaces, and thin films – 74.25.Gz Optical properties – 78.66.Jg Amorphous semiconductors; glasses

1 Introduction

In recent years, considerable attention has been focused on amorphous semiconductors, especially those known as chalcogenide glasses, due to their threshold and memory switching behavior and the infrared transmission of many of these glasses which make them potential materials for industrial applications in memory devices and fiber optics [1,2]. Structural studies of chalcogenide glasses are important in determining the transport mechanism, thermal stability and practical applications. Different techniques have been used to study the structure of chalcogenide glasses, e.g. electron microscopy, X-ray diffraction and differential scanning calorimetry [3–5]. Selenium is selected because of its wide commercial applications. Its device applications like switching, memory and xerography, etc. makes it attractive. It also exhibits a unique property of reversible transformation [6]. This property makes it very useful in optical memory devices. But in pure state it has disadvantages because of its short lifetime and low sensitivity. To overcome these difficulties, certain additives are used such as Ge, Sn, Sb, Te, Pb, Bi, In, etc. These materials are generally p-type semiconductors. However, when bismuth impurities are added in large concentrations (11 at%, 7 at% and 3.5 at% in Ge–S, Ge–Se and Ge–Te, respectively), they exhibit carrier sign reversal [7–9]. Carrier sign reversal has also been observed in liquid alloys Ge–Te–M (M = Tl or Bi) for Bi concentrations between 5–10 at% [10].

Thermal annealing has pronounced effects on the electrical and optical properties due to structural relaxation/transformation. In the present work, a study on the effect of thermal relaxation process with composition on the physical properties in the multi-component amorphous $Sn_{10}Sb_{20-x}Bi_xSe_{70}$ ($0 \leqslant x \leqslant 8$) chalcogenide system has been undertaken. The compositional dependence of the optical energy gap has also been investigated. The effects of thermal annealing (below the glass transition temperature for 1 h) on the optical properties as well as on the structure of the films are also reported.

2 Experimental

Bulk samples of $Sn_{10}Sb_{20-x}Bi_xSe_{70}$ ($0 \leqslant x \leqslant 8$) were prepared by conventional melt quenching technique. The film deposition was carried out in a high vacuum system (HINDHIVAC coating unit, Model No. 12A4D) in a pressure of 10^{-5} mbar. The films were deposited on well-cleaned glass slides kept at room temperature as substrates and with source material taken in a molybdenum boat. A Philips X-ray diffractometer (type PW3710 mpd with a PW1830 generator) was used to identify the amorphous/crystalline phases in the pristine and annealed films. The surface morphology of the pristine and annealed films was analyzed using a scanning electron microscope (SEM) (Philips XL30 ESEM system) operated

[a] e-mail: rthangaraj@rediffmail.com

Table 1. Values of thickness (d), glass transition temperature (T_g) at 20 K/min heating rate, optical gap (E_g^{opt}), activation energy (E_d) and band tailing parameter B^{-1} for the pristine as well as annealed thin films of the $Sn_{10}Sb_{20-x}Bi_xSe_{70}$ ($0 \leqslant x \leqslant 8$) system.

x (at%)	d (nm)	T_g (K)	E_g^{opt} (eV) pristine	E_g^{opt} (eV) annealed	E_d (eV) pristine	E_d (eV) annealed	B^{-1} (cm eV) pristine	B^{-1} (cm eV) annealed
0	1273	429	1.19	1.22	0.45	0.42	578.57	567.25
2	1079	431	1.23	1.14	0.47	0.39	593.02	562.72
4	1250	436	1.03	0.85	0.29	0.27	440.49	322.79
6	1250	437	1.01	0.74	0.24	0.20	380.33	254.98
8	1169	438	0.99	0.71	0.22	0.16	401.90	246.65

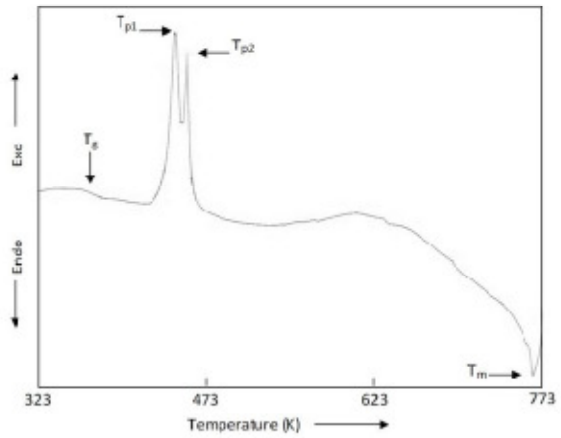

Fig. 1. Typical DSC thermograms for the $Sn_{10}Sb_{18}Bi_2Se_{70}$ sample at 20 K/min heating rate.

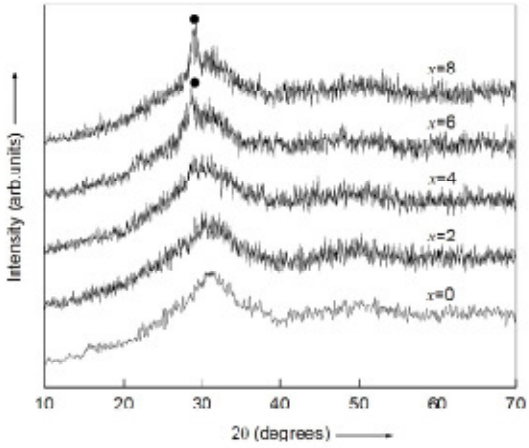

Fig. 2. The X-ray diffraction patterns for the pristine films of $Sn_{10}Sb_{20-x}Bi_xSe_{70}$ ($0 \leqslant x \leqslant 8$) system.

at 20 kV. Thickness was measured by KLA Tencor P15 surface profiler and the obtained values for all the films are reported in Table 1. The differential scanning calorimetric (DSC) studies were carried out to know the glass transition temperature and a temperature of ~25 K below the glass transition temperature was used for annealing (393 K, 400 K, 405 K, 413 K, and 417 K respectively). The annealing of the films was performed in a running vacuum (~10^{-5} mbar) with a heater and thermocouple connections for temperature measurement. The conductivity measurements were carried out in the temperature range 233–343 K in a running vacuum of ~10^{-4} mbar. Electrical contacts with an electrode gap of ~2 mm in a coplanar geometry were made by pre-deposition of aluminum. The current was measured using a digital picoammeter (DPM-111 Scientific Equipments, Roorkee). The optical transmission spectrum was recorded at room temperature for all the samples using UV-visible spectrophotometer (VARIAN Cary500 UV-VIS-NIR) in the wavelength range of 400–3000 nm. The optical energy gap was obtained from a plot of $(\alpha h\nu)^{1/2}$ vs. $h\nu$ and taking the intercept of the straight line portion of the curve on the energy axis, where α is the absorption coefficient.

3 Results and discussion

3.1 Thermal and structural properties

Figure 1 shows a typical DSC scan for a $Sn_{10}Sb_{18}Bi_2Se_{70}$ sample at 20 K/min heating rate. The glass transition temperature, two peak crystallization temperatures and the melting temperature are observed for this sample. The presence of two exothermic peaks means that there are two phases appearing during the crystallization process. The glass transition temperature (T_g) shifts towards higher temperature as the Bi content increases as well as with the increase in heating rate. The values of T_g at a heating rate of 20 K/min for all the samples investigated are listed in Table 1. The change in the value of T_g can be explained on the basis of chemically ordered network (CON) model [11]. Figure 2 shows the X-ray diffractograms for the pristine $Sn_{10}Sb_{20-x}Bi_xSe_{70}$ ($0 \leqslant x \leqslant 8$) thin films. The absence of sharp peaks for the samples with $x = 0$, 2, 4 at% of Bi show the amorphous nature of these films. The samples with $x = 6$ and 8 show a small peak revealing the presence of small amount of some crystalline phase in the amorphous matrix. This peak is identified from the

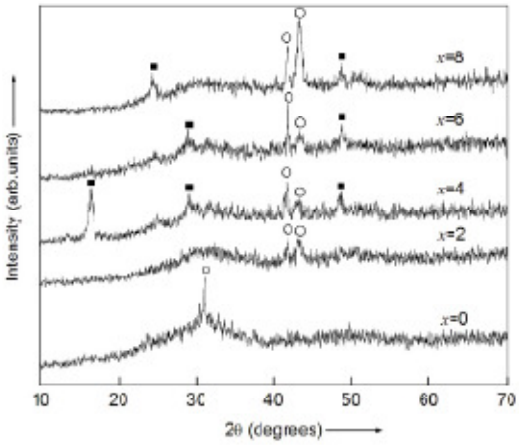

Fig. 3. The X-ray diffraction patterns for the annealed $Sn_{10}Sb_{20-x}Bi_xSe_{70}$ ($0 \leqslant x \leqslant 8$) films.

JCFDS data base (1997) as due to the formation Bi_2Se_3 (■) phase. Figure 3 shows the X-ray diffractograms for all the films annealed below the glass transition temperature (393 K, 400 K, 405 K, 413 K, and 417 K respectively) for 1 h. The sample with $x = 0$ Bi concentration has only one peak which corresponds to Sb_2Se_3 (□) phase as identified from the JCPDS files. The number of peaks increase for the samples with Bi concentration $x = 2, 4, 6, 8$ which indicates the micro-crystallization of the amorphous films after annealing below the glass transition temperature for 1 h. These peaks are identified as due to the formation of Bi_2Se_3 (○) and $BiSe_2$ (■) phases.

The morphology of the $Sn_{10}Sb_{18}Bi_2Se_{70}$ thin film annealed at 400 K for 1 h was examined using scanning electron microscope (SEM). Figures 4a, 4b shows the surface microstructure of the pristine as well as annealed films. As observed from Figure 4a for the pristine film, the surface appears smooth having featureless background which means that for $x = 2$ at%, the system remains amorphous which is already confirmed from the X-ray diffractograms. After 1 h annealing at $T = 400$ K, polycrystalline structures of different shapes embedded in the amorphous matrix were observed as shown in Figure 4b. These phases may be due to the formation of Bi_2Se_3 and $BiSe_2$ as identified from the X-ray diffractograms.

3.2 Optical properties

In order to determine the absorption coefficient (α) of the films versus the incident energy, transmission and reflection measurements were carried out at room temperature. In amorphous semiconductors, the optical absorption spectrum has been found to have three distinct regions viz., a high absorption region, the exponential edge region, and a weak absorption tail that originates from the defects and impurities. The high absorption part

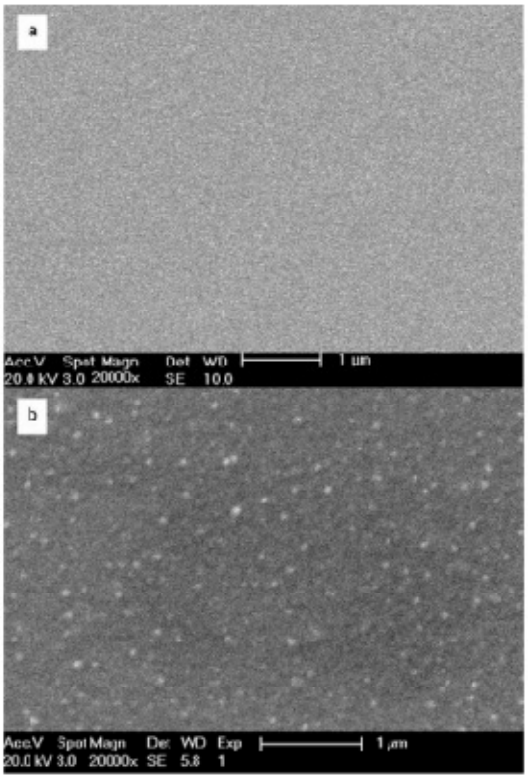

Fig. 4. SEM micrographs (a) for the pristine and (b) annealed at 400 K for 1 h for $Sn_{10}Sb_{18}Bi_2Se_{70}$ film.

is caused by the band to band transition and is followed by an exponential Urbach tail and then finally, a weak absorption tail. It is well known that the weak absorption tail originates from the defects and impurities and the exponential region is strongly related to the characteristic structural randomness of amorphous material, whereas, the high absorption region determines the optical energy gap. The absorption coefficient α was computed from the experimental measured values of R and T according to the following expression

$$T = (1 - R)^2 \exp(-\alpha d)$$

where d is the thickness of the investigated films. In the high absorption region ($\alpha \geqslant 10^4$ cm^{-1}), photon energy dependence of absorption coefficient can be described according to a model proposed by Tauc [12]. The model is

$$(\alpha h\nu) = B(h\nu - E_g)^2$$

where B is a constant which depends upon the transition probability and E_g is the optical band gap. Figures 5 and 6 show a plot of $(\alpha h\nu)^{1/2}$ versus $(h\nu)$ for the pristine as well as annealed thin films for different Bi concentrations of $Sn_{10}Sb_{20-x}Bi_xSe_{70}$ ($0 \leqslant x \leqslant 8$) system.

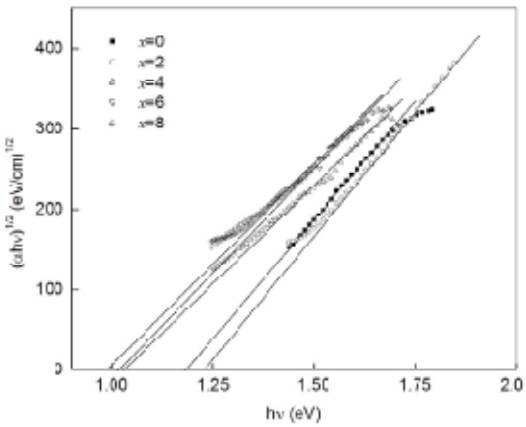

Fig. 5. Plot showing the variation of $(\alpha h\nu)^{1/2}$ with $(h\nu)$ for the pristine $Sn_{10}Sb_{20-x}Bi_xSe_{70}$ $(0 \leqslant x \leqslant 8)$ films.

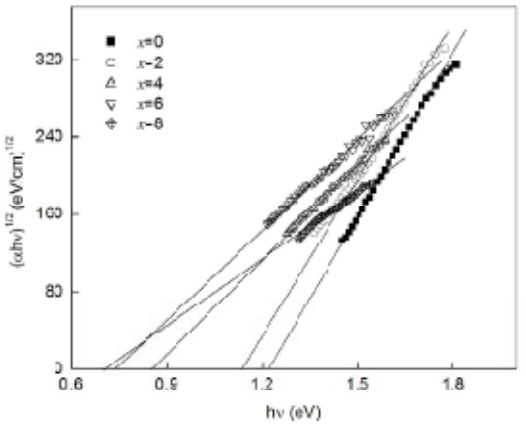

Fig. 6. Plot showing the variation of $(\alpha h\nu)^{1/2}$ with $(h\nu)$ for the annealed $Sn_{10}Sb_{20-x}Bi_xSe_{70}$ $(0 \leqslant x \leqslant 8)$ films.

The optical band gap (E_g) is calculated by taking the intercept on the energy axis. The variation of the optical gap with Bi concentration for the pristine and annealed films is listed in Table 1. As observed from Table 1, the optical gap for the pristine films initially increases with $x = 2$ Bi concentration and then decreases sharply for all the samples. For the annealed films, the optical gap initially increases for $x = 0$ at% as compared to the unannealed sample and then decreases sharply for all the samples with increase of Bi and is less as compared to the unannealed films. The homogeneous mixing at lower concentrations and the formation of strong Bi–Se bonds in the network, with consequent decrease in the defect states may be the reason for initial increase in the optical gap. Due to the increase in Bi content, the formation of Bi rich backbone clusters in the network are enhanced. Therefore, more addition of Bi causes an increase in the size of these clusters, which due to lower thermal conductivity of amorphous network, causes it to crystallize in the network. Their nucleation and growth with increase in Bi content enhances the defect states associated with the inhomogeneous two phase system or the constraint to the mixing of crystalline bismuth clusters and amorphous network. The increase of these defect states may thus lead to decrease in the optical gap. However, the typical role played by Bi impurity in chalcogenide systems, i.e. the change in conduction type from p-type to n-type also influences the optical properties of the system. The sharp change in the optical gap at higher Bi content may also be due to the occurrence of carrier type reversal (CTR) in the present system [13,14]. The change in the optical band gap for the annealed films with increase in Bi content from $x = 0$ to 8 may be due to the rearrangement of localized defect states, D^+ and D^- (which are characteristic defects of chalcogenide glasses), induced by thermal annealing below T_g [15]. The quantity B^{-1}, which is determined from the slope of the Tauc plots of $(\alpha h\nu)^{1/2}$ versus $(h\nu)$ for the $Sn_{10}Sb_{20-x}Bi_x$–Se_{70} $(0 \leqslant x \leqslant 8)$ system for all the pristine as well as annealed films, can be taken as an approximate measure of the extent of band tailing into the band gap of the amorphous semiconductors. The obtained values of B^{-1} for the pristine as well as annealed films are listed in Table 1. As observed from Table 1, the values of B^{-1} for the pristine films do not show any particular trend with Bi concentration but in case of annealed films the values of B^{-1}decrease with increase in Bi content for all the samples. The rise and fall in the value of B^{-1} may be attributed to a decrease in the extent of localized tail states and due to the development of defect states by the addition of Bi.

3.3 Electrical properties

The dc conductivity measurements yield valuable information about the conduction mechanism in amorphous semiconductors. Chalcogenide glasses normally show an activated temperature dependent dark conductivity according to the Arrhenius relation

$$\sigma = \sigma_0 \exp \frac{-E_d}{KT},$$

where σ_0 is the material related pre-exponential factor, E_d is the activation energy for dc conduction and is calculated from the slope of $\ln(\sigma)$ versus $1000/T$ plots, k is the Boltzmann constant and T is the absolute temperature. Figure 7 shows the variation of $\ln(\sigma)$ with temperature for the pristine as well as annealed films and these plots are found to be straight lines indicating that the conduction is through an activated process having single activation energy in the temperature range 233–343 K. The dark conductivity of all the samples increase with increase in temperature for both the pristine and annealed films as shown in Figure 7. The obtained values of the activation energy for both the pristine and annealed films are listed in Table 1. As observed from Table 1, for the pristine films at low Bi concentration, there is a little change in activation energy where as at higher concentrations of Bi

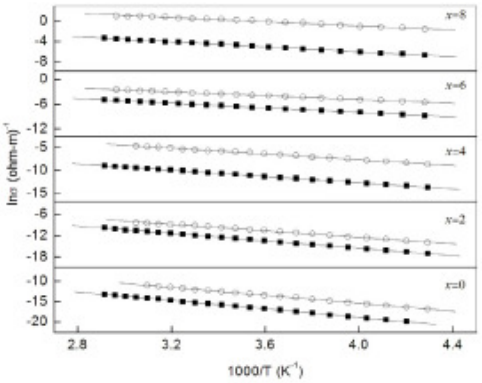

Fig. 7. Plots of $\ln(\sigma)$ versus $1000/T$ for the pristine (■) as well as annealed (◯) $Sn_{10}Sb_{20x}Bi_xSe_{70}$ ($0 \leqslant x \leqslant 8$) films.

a considerable decrease in the activation energy is observed. For the annealed films, the activation energy is less as compared to the unannealed films and decreases substantially with the increase in Bi content for all the samples. With the addition of Bi, there is an increase in the ionic bonds (Bi–Se). Moreover, the larger polarizability of the dopants helps in the formation of partially ionic bonds with chalcogen likely and also accounts for the increase in conductivity. The sudden decrease in activation energy can be understood by considering the effect of charged impurities on the defect density and carrier concentration. According to Mott and Davis [16], the increase in the density of localized states leads to the formation of compositions with a high degree of disorder. The variation of dc parameters with Bi for the investigated compositions may be explained by assuming that Bi atoms act as impurity centers (give rise to some non-radiative defect centers) in the mobility gap. This induces structural changes in the network which may disturb the balance of the charged defects and consequently change the electric conduction. In such a situation the distribution and density of localized states are modified and even some new trap states can be created in the mobility gap [17]. Addition of Bi brings about a reduction in the relative concentration of D^+ as compared with D^- defects. This imbalance accompanied by the contribution of extra electrons brings about dominant electron conduction in Bi doped glasses. Also the thermal annealing seems to readjust the localized states in such a way that there is a substantial decrease in the value of activation energy.

4 Conclusion

Thin films of Sn–Sb–Bi–Se were deposited at room temperature have shown amorphous nature as confirmed from the X-ray diffractograms for $x = 0, 2, 4$ pristine films and the samples with $x = 6, 8$ at% of Bi show small peak. The binary phases of Bi_2Se_3 and $BiSe_2$ were resulted after heat treatment for 1 h below the glass transition temperature. Scanning electron microscopy studies also show the presence of polycrystalline phases in the amorphous matrix after annealing. Optical gap initially increases for lower Bi content and then decreases sharply for the pristine films as Bi content increases. After heat treatment, the optical gap increases for $x = 0$ as compared to the pristine film and then decreases for all the samples as Bi content increases. The activation energy follows the same trend with Bi concentration as that of the optical gap.

References

1. P. Nermec, M. Frumar, B. Frumarova, M. Jelinek, J. Lancok, J. Jedelsky, Opt. Mat. **15**, 191 (2000)
2. P. Nermec, M. Frumar, J. Jedelsky, M. Jelinek, J. Lancok, I. Gregora, J. Non-Cryst. Sol. **1013**, 299 (2002)
3. R.M. Mehra, R. Kumar, P.C. Mathur, Thin Solid Films **15**, 170 (1989)
4. J. Nishi, S. Morimoto, I. Ingawa, R. Iizuka, T. Yamashita, J. Non-Cryst. Sol. **140**, 199 (1992)
5. J.A. Savage, *Infrared Optical Materials and their Antireflection Coatings* (Adam Hilger, Bristol, 1985)
6. K. Tanaka, Phys. Rev. B **39**, 1270 (1989)
7. N. Toghe, T. Minami, Y. Yamamoto, M. Tanaka, J. Appl. Phys. **51**, 1048 (1980)
8. P. Nagaels, L. Tichy, A. Triska, H. Ticha, J. Non-Cryst. Sol. **59**, 1015 (1983)
9. K.L. Bhatia, G. Parthasarthy, A.K. Sharma, E.S.R. Gopal, Philos. Mag. B **73**, 383 (1996)
10. H. Hiroshi, N. Yoshi, J. Phys. A: Condens. Matter **5**, 8523 (1993)
11. M. Ahmad, P. Kumar, N. Suri, J. Kumar, R. Thangaraj, Appl. Phys. A **94**, 933 (2009)
12. J. Tauc, *Amorphous and Ligiud Semiconductors* (Plenum Press, New York, 1974), p. 172
13. N. Tohge, Y. Yamamoto, T. Minami, M. Tanaka, Appl. Phys. Lett. **34**, 640 (1979)
14. N. Tohge, M. Minami, T. Tanaka, J. Non-Cryst. Sol. **283**, 38 (1980)
15. N.F. Mott, E.A. Davis, R.A. Street, Philos. Mag. **32**, 961 (1975)
16. N.F. Mott, E.A. Davis, *Electronics Process in Non-Crystalline Materials* (Clarendon Press, Oxford, 1971), p. 327
17. D. Adler, M.S. Shur, M. Silver, S.R. Ovshinsky, J. Appl. Phys. **51**, 3289 (1980)